PHYSICAL REVIEW B **84**, 140409(R) (2011)

Effects of cation-size variance on spin and orbital orders in $Eu_{1-x}(La_{0.254}Y_{0.746})_xVO_3$

R. Fukuta,[1] S. Miyasaka,[1] K. Hemmi,[1] S. Tajima,[1] D. Kawana,[2] K. Ikeuchi,[2] Y. Yamasaki,[2] A. Nakao,[2] H. Nakao,[2] Y. Murakami,[2] and K. Iwasa[3]

[1]*Department of Physics, Osaka University, Osaka 560-0043, Japan*

[2]*Condensed Matter Research Center and Photon Factory, Institute of Materials Structure Science, High Energy Accelerator Research Organization, Tsukuba 305-0801, Japan*

[3]*Department of Physics, Tohoku University, Sendai 980-8578, Japan*

(Received 5 August 2011; revised manuscript received 4 October 2011; published 24 October 2011)

We have investigated the R-ion (R = rare earth or Y) size variance effect on spin/orbital order in $Eu_{1-x}(La_{0.254}Y_{0.746})_xVO_3$. The size variance disturbs one-dimensional orbital correlation in C-type spin/G-type orbital ordered states and suppresses this spin/orbital order. In contrast, it stabilizes the other spin/orbital order. The results of neutron and resonant x-ray scattering denote that in the other ordered phase, the spin/orbital patterns are G type/C type, respectively.

DOI: 10.1103/PhysRevB.84.140409 PACS number(s): 75.25.Dk, 71.30.+h, 75.30.Kz

Perovskite-type transition-metal oxides RMO_3 (R = rare-earth elements or Y, M = transition-metal ones) and the electron- and hole-doped systems show many attractive physical properties related with d electrons and have been investigated extensively.[1] In RMO_3, electronic and magnetic states can be changed by controlling the M-O-M bond angle, doping carrier, applying magnetic and electric fields, and so on.[1,2] Among these, the M-O-M bond angle is systematically dependent on the R-site ionic radius.[3] On the other hand, the structural disorder caused by the size mismatch of the R-site cations is also used as a controllable parameter.[2,4–7] We describe this disorder as the "size variance (SV)," expressed by $\langle r_i^2\rangle - \langle r_i\rangle^2$ (r_i is the R-site ionic radius). In general, the SV suppresses the long-range spin, charge, and orbital order, and consequently the critical temperature (T) decreases with increasing SV.[2,4] In nearly half doped manganites, the SV effect induces the suppression of long-range charge/orbital order (CO/OO) and the ferromagnetic order. As a result, the manganites undergo the phase transition from the long-range CO/OO insulator or ferromagnetic metal to a spin-glass insulator.[4] In this Rapid Communication, we report on the observation of rare phenomena that the SV induces instability of one spin/orbital ordered state but stabilizes the other one in RVO_3. This system consequently shows the spin/orbital phase transition from one long-range order to the other long-range order by changing SV. The phase transition between the two types of spin/orbital long-range orders in RVO_3 induced by SV is quite different from those in the manganites, where the phase transition from long-range spin/charge/orbital ordered states to short-range ordered ones occurs by an increase of SV.

RVO_3 is one of the prototypical systems with spin and orbital degrees of freedom of t_{2g} electrons. There are two electrons in the $3d$ orbitals of V^{3+}. One electron always occupies the d_{xy} orbital due to the symmetry-lowered crystal field by the orthorhombic distortion, which is coupled ferromagnetically to the other electron in either a d_{yz} or d_{zx} orbital through Hund's rule coupling. RVO_3 shows two types of the spin/orbital order concomitantly with the structural phase transition, i.e., C-type spin order (C-SO)/G-type orbital order (G-OO) with a $P2_1/b$ monoclinic structure, and G-SO/C-OO with a $Pbnm$ orthorhombic structure.[8–13] In C-OO the electronic configurations of $d_{xy}^1d_{yz}^1/d_{xy}^1d_{zx}^1$ are alternately arranged in the ab plane and are identical along the c axis [Fig. 1(a)], while in G-OO those are alternately arranged in all three directions [Fig. 1(b)]. C-type/G-type SO patterns are shown in the same manner as the OO, as presented in Figs. 1(a) and 1(b). The transition T of each SO/OO show a systematic dependence on the r_i.[13] On the other hand, Yan and co-workers investigated the SV effect on the spin and orbital orders in RVO_3.[14] They melt-grew $Y_{1-x}(La_{0.2337}Lu_{0.7663})_xVO_3$ polycrystals, where the average r_i is fixed to be the same as that of Y^{3+}. In this system, the change in the V-O-V bond angle is vanishingly small, while the variance linearly increases with x. With increasing x, the transition T of G-SO/C-OO is enhanced while those of C-SO/G-OO are suppressed. Their results have also suggested that in large variance region, there is only one magnetically ordered state. But, to the best of our knowledge, there is little information about this state.

In RVO_3, the SV of R ions seems not only to destabilize one long-range SO/OO, but also to stabilize the other order. To clarify the SV effect in this t_{2g} orbital system, we have investigated the SO/OO in a $Eu_{1-x}(La_{0.254}Y_{0.746})_xVO_3$ single crystal. The pure material ($x = 0$) $EuVO_3$ undergoes one pattern of SO/OO order, i.e., a structural phase transition from orthorhombic to monoclinic lattices accompanied with G-OO at 204 K and also a magnetic transition from paramagnetic to C-SO at 131 K, as T is lowered.[15,16] This compound is located near the phase boundary between two SO/OO states. So we expected that if the large SV actually stabilizes the G-SO/C-OO, the G-SO/C-OO would appear in $Eu_{1-x}(La_{0.254}Y_{0.746})_xVO_3$. In this compound, the average ionic radius of $(La_{0.254}Y_{0.746})^{3+}$ is the same as that of Eu^{3+}, and the variance linearly increases with x. Here, the ionic radii for 12 coordination are 1.228, 1.360, and 1.183 Å for Eu^{3+}, La^{3+}, and Y^{3+}, respectively.[17] The choice of this mixed crystal of $EuVO_3$ and $(La_{0.254}Y_{0.746})VO_3$ enables us to systematically investigate the spin/orbital phase diagram with varying the SV, while avoiding the large influence of the $4f$ moment on V $3d$ spins because of small magnetic moment for Eu^{3+}, and no magnetic La^{3+} and Y^{3+}.[16,20] In this Rapid Communication, we have measured the magnetization (M), heat capacity (C), lattice constants, resonant x-ray scattering (RXS), and neutron diffraction (ND) to clarify the spin/orbital patterns and the phase diagram of RVO_3 with changing the SV.

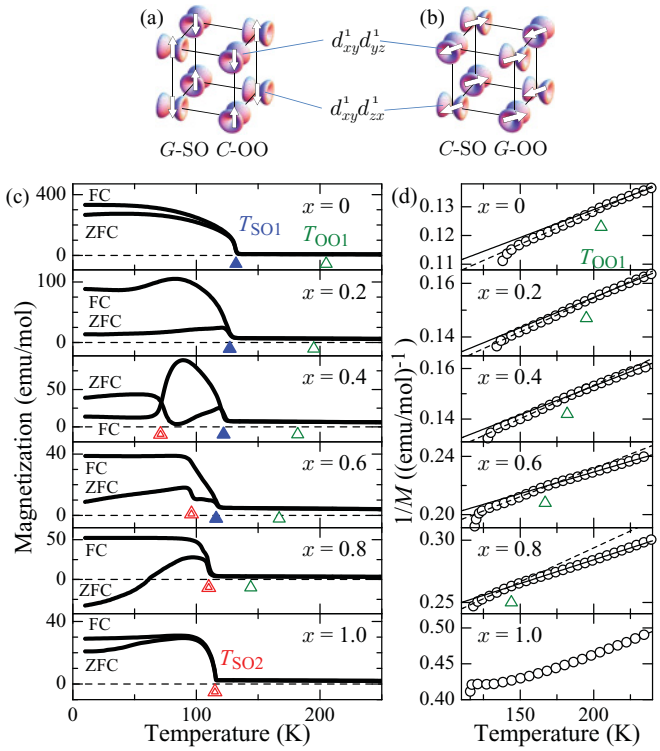

FIG. 1. (Color online) Schematic views of spin (arrows) and orbital order: (a) *G*-SO/*C*-OO and (b) *C*-SO/*G*-OO. (c) T-dependent M for $Eu_{1-x}(La_{0.254}Y_{0.746})_xVO_3$ with applied 1 kOe in zero-field-cooling (ZFC) and field-cooling (FC) processes. The open green, closed blue, and double red triangles indicate T_{OO1}, T_{SO1}, and T_{SO2}, respectively. (d) $1/M$ as a function of T for these compounds. Except for $x = 1.0$, the dashed lines represent the Curie-Weiss fitting between T_{SO1} and T_{OO1}, and solid lines above T_{OO1}.

All the samples of $Eu_{1-x}(La_{0.254}Y_{0.746})_xVO_3$ were single crystals grown by a floating-zone method.[21] The R concentrations of the grown crystals were confirmed to be the same as the nominal ones by an inductively coupled plasma (ICP) analysis. M measurements were carried out with a superconducting quantum interference device (SQUID) magnetometer. C measurements were performed by the relaxation method. The lattice constants were measured by powder x-ray scattering techniques using an x-ray with an energy of 15 keV at BL-8A of Photon Factory (PF), KEK, Japan. The structural parameters were determined by a Rietveld analysis using the RIETAN-FP package.[22] All the peaks of powder x-ray diffraction profiles for $x = 0$, 0.4, and 1.0 can be well fitted by using the structural parameters of the $Pbnm$ orthorhombic or the $P2_1/b$ monoclinic lattices, and do not show any broadening and splitting. The results indicate that this system has no unique structural phase and no phase separation. The RXS measurements for single crystals of $x = 1.0$ with a (100) surface were performed at BL-4C of PF. In order to analyze whether the polarization of the scattering beam is parallel (π' polarization) or perpendicular (σ' polarization) to the scattering plane, we used a pyrolitic graphite (004) crystal. The ND measurements for the single crystal with $x = 1.0$ were performed by using the triple-axis spectrometers of thermal neutron TOPAN (6G), which are installed in the research reactor JRR-3 of Japan Atomic Energy Agency, Tokai.

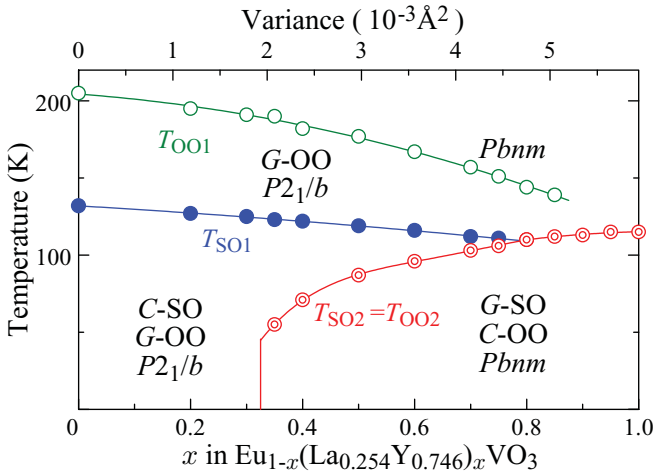

FIG. 2. (Color online) Spin/orbital phase diagram of $Eu_{1-x}(La_{0.254}Y_{0.746})_xVO_3$. Open green, closed blue, and double red circles indicate the transition T_{OO1}, T_{SO1}, and $T_{SO2} = T_{OO2}$, respectively. The top axis shows the variance of the ionic radius on the rare-earth site.

The T dependence of M and its inverse ($1/M$) for $Eu_{1-x}(La_{0.254}Y_{0.746})_xVO_3$ with various x are shown in Figs. 1(c) and 1(d). As shown in Fig. 1(d), the M except for $x = 1.0$ follows the Curie-Weiss rule in the paramagnetic phase. The slope of $1/M$ changes at the transition T of *G*-OO (T_{OO1}).[23] In Fig. 1(c), M of $EuVO_3$ ($x = 0$) shows a significant jump at 132 K, which we assigned as the transition T of *C*-SO (T_{SO1}).[15,16] The same magnetic transition has been observed below $x \sim 0.8$. In addition, an anomaly in T-dependent M, which we defined as T_{SO2}, appears in the samples with $x \sim 0.4$, and T_{SO2} increases with x. At T_{SO2}, the antiferromagnetic spin pattern is changed from C type to the other one, as described later. With increasing x, the magnitude of M at low T decreases, which may be related with the decrease of magnetic Eu^{3+}.

Figure 2 presents the spin/orbital phase diagram of $Eu_{1-x}(La_{0.254}Y_{0.746})_xVO_3$ determined by the results in Figs. 1(c) and 1(d). T_{OO1} and T_{SO1} decrease with increasing x and vanish above $x \sim 0.8$. As described later, the anomaly in Fig. 1 accompanies not only the *G*-SO but also the *C*-OO, and this transition T ($T_{SO2} = T_{OO2}$) appears above $x \sim 0.4$ and is gradually enhanced with x. This suggests that the *G*-SO/*C*-OO is stabilized by the SV. With further increasing x, only *G*-SO/*C*-OO exists near $x = 1.0$.

Figure 3 shows the T dependence of lattice constants a,b,c as well as M and C for $x = 0$, 0.4, and 1.0 samples.[24] At T_{OO1}, the T dependence of lattice constants has kinks, and the C has a peak, indicating the structural phase transition from the orthorhombic $Pbnm$ to monoclinic $P2_1/b$ lattices concomitantly with the *G*-OO as T decreases [Figs. 3(a), 3(b), 3(d)–3(f), and 3(h)]. On the other hand, the anomaly of M and the peak of C at T_{SO1} indicate the magnetic transition to *C*-SO [Figs. 3(c), 3(d), 3(g), and 3(h)]. As shown in Figs. 3(e)–3(l), lattice constants M and C have anomalies at $T_{SO2} = T_{OO2}$ for $x = 0.4$ and 1.0 samples. These results reveal that the magnetic and structural phase transitions occur together at T_{SO2}. The changes in lattice constants are very similar to the orbital phase

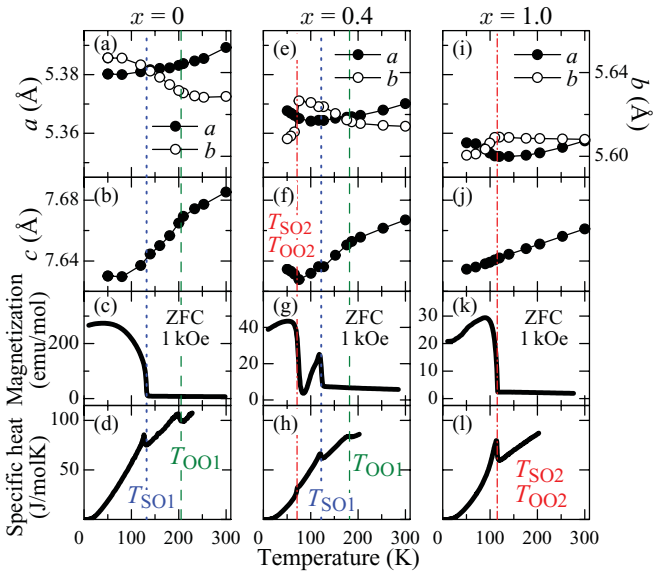

FIG. 3. (Color online) T dependence of the lattice constants a and b [(a), (e), (i)], c [(b), (f), (j)], M measured in 1 kOe after ZFC [(c), (g), (k)], and C [(d), (h), (l)] for $Eu_{1-x}(La_{0.254}Y_{0.746})_xVO_3$ with $x = 0$, 0.4, and 1.0. Vertical dashed green, dotted blue, and dashed-dotted red lines indicate T_{OO1}, T_{SO1}, and $T_{SO2} = T_{OO2}$, respectively.

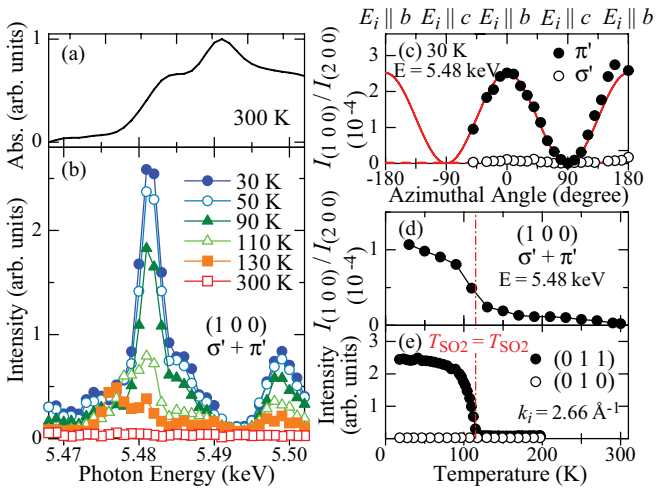

FIG. 4. (Color online) Diffraction results for an $x = 1.0$ sample of $Eu_{1-x}(La_{0.254}Y_{0.746})_xVO_3$. (a) X-ray absorption spectrum at 300 K. (b) Photon-energy spectra of the $\sigma' + \pi'$ component of (100) orbital reflection at various T. The incident beam has σ polarization and E_i is parallel to the b axis. (c) Closed and open circles indicate the intensity of the π' and σ' components of (100) reflection normalized by the (200) fundamental one as a function of the azimuthal angle. The red solid and dashed lines are model calculations for C-OO of the π' and σ' components. (d) T dependence of intensity of the $\sigma' + \pi'$ component of the normalized (100) reflection at 5.48 keV. Vertical lines indicate $T_{SO2} = T_{OO2}$. (e) T dependence of intensity of (011) and (010) magnetic Bragg reflections, indicated by closed and open circles, respectively. $k_i = 2.66$ Å^{-1} is the momentum of incident neutrons.

transition to C-OO.[25] These behaviors suggest the existence of the lower-T orthorhombic phase with the C-OO (and coupled to G-SO).

To confirm the pattern of SO/OO at the ground state above $x = 0.35$, we performed the RXS and ND measurements for the $x = 1.0$ sample. Figure 4(a) shows the x-ray absorption spectrum at 300 K for $x = 1.0$. The rising of the absorption spectrum near 5.48 keV is due to the V K main edge. Figure 4(b) shows the energy dependence of the intensity of (100) orbital reflection at various T. This reflection does not obey the extinction rule but corresponds to the propagation vectors for C-OO. The symmetry of the degenerated orbital states at each V^{3+} site can be investigated through the azimuthal angle dependence of the orbital reflections. As shown in Fig. 4(c), the (100) reflection normalized by the (200) fundamental one at the main edge is maximum with the electric vector of incident beam $E_i \parallel b$ configuration and nearly vanishes with $E_i \parallel c$. Model calculations for π' and σ' components in C-OO are also shown in Fig. 4(c). (In a simple G-OO model, the π' and σ' components are equal to zero.) In our calculations, the atomic scattering tensor of each V^{3+} ion is the same as that in Ref. 11 and the structural distortion, estimated by the Rietveld analysis for $x = 1.0$, is considered. The good agreement between the experimental and calculated data of each component, shown in Fig. 4(c), indicates the existence of C-OO.

Figure 4(d) displays the T dependence of the normalized intensity of the (100) orbital reflection with the $E_i \parallel b$ configuration at the main edge in a warming run. Figure 4(e) demonstrates a comparison between T dependences of the integrated intensity of (011) and (010) magnetic Bragg reflections measured by ND in a warming run. The (011) reflection is caused by the G-SO, and the (010) is caused by the C-SO.[8] The intensity of the (100) orbital reflection and (011) magnetic Bragg reflection are suddenly reduced at approximately $T_{SO2} = T_{OO2}$ as T is increased. These results indicate that the G-SO/C-OO occurs below $T_{SO2} = T_{OO2}$ in the $x = 1.0$ sample. The intensity of (100) orbital reflection remains finite even above $T_{SO2} = T_{OO2}$, which is caused by the C-OO fluctuation and perhaps the RXS component from the local crystal symmetry of space group $Pbnm$.

The SV generally suppresses the long-range order of spin, orbital, and charge. The gradual decrease of T_{OO1} and T_{SO1} with the variance reveals that the SV destabilizes C-SO/G-OO in $Eu_{1-x}(La_{0.254}Y_{0.746})_xVO_3$. However, the appearance of G-SO/C-OO and the increase of $T_{SO2} = T_{OO2}$ with increasing the SV cannot be explained by the general scenario. To account for this anomalous behavior of G-SO/C-OO, one may remember the R-site covalency effect.[25–27] In $Eu_{1-x}(La_{0.254}Y_{0.746})_xVO_3$, however, the R-site covalency is almost constant, because the average ionic radius of the R site is unchanged.

On the other hand, the competition of two SO/OO states in RVO_3 is emphasized.[27] Among these states, the C-SO/G-OO includes the quasi-one-dimensional (quasi-1D) orbital chain along the c axis, which is described by a quasi-1D model for the orbital pseudospin ($\tau = 1/2$). This quasi-1D antiferroic orbital chain strongly enhanced the quantum orbital fluctuation, and causes a 1D optical response and the orbital excitation.[21,28–32] When the SV increases, the 1D orbital chain is easily deranged, and the 1D orbital correlation (orbital order and fluctuation) is suppressed. As a result, the C-SO/G-OO is destabilized

but the other competing SO/OO, *G*-SO/*C*-OO, is relatively stabilized. Therefore, in the present systems the ground state is changed from *C*-SO/*G*-OO to *G*-SO/*C*-OO and $T_{SO2} = T_{OO2}$ is gradually enhanced with x. The *G*-SO/*C*-OO phase only exists at approximately $x = 1.0$ in this system, while the SV-free $R\mathrm{VO_3}$ always has the *C*-SO/*G*-OO at low T.[13] This difference between the present system and $R\mathrm{VO_3}$ without the *R*-ion SV indicates that the destruction of the 1D orbital chain by SV of *R* ions plays an important role of the disappearance of *C*-SO/*G*-OO.

We have clarified the spin/orbital phase diagram for $\mathrm{Eu}_{1-x}(\mathrm{La}_{0.254}\mathrm{Y}_{0.746})_x\mathrm{VO_3}$ with controllable cation SV by changing x. By increasing SV, *G*-OO and *C*-SO tend to be destabilized, while the other ordered phase is stabilized. We confirmed that this spin/orbital ordered state is the *G* type/*C* type by using ND and RXS measurements, respectively. The SV disturbs the 1D orbital chain in the state. The suppression of the 1D orbital correlation causes the phase transition from *C*-SO/*G*-OO to *G*-SO/*C*-OO states.

This study has been approved by the PF Program Advisory Committee (No. 2009S2-008). The ND measurement was performed under the User program conducted by ISSP, University of Tokyo (No. 10402).

[1] M. Imada, A. Fujimori, and Y. Tokura, Rev. Mod. Phys. **70**, 1039 (1998).
[2] Y. Tokura, Rep. Prog. Phys. **69**, 797 (2006).
[3] D. A. MacLean, H. Ng, and J. E. Greedan, J. Solid State Chem. **30**, 35 (1979).
[4] Y. Tomioka and Y. Tokura, Phys. Rev. B **70**, 014432 (2004).
[5] L. M. Rodriguez-Martinez and J. P. Attfield, Phys. Rev. B **54**, 15622 (1996).
[6] J. P. Attfield, A. L. Kharlanov, and J. A. McAllister, Nature (London) **394**, 157 (1998).
[7] P. V. Vanitha *et al.*, Chem. Mater. **12**, 1666 (2000).
[8] H. Kawano, H. Yoshizawa, and Y. Ueda, Phys. Soc. Jpn. **63**, 2857 (1994).
[9] C. Ulrich *et al.*, Phys. Rev. Lett. **91**, 257202 (2003).
[10] M. Reehuis *et al.*, Phys. Rev. B **73**, 094440 (2006).
[11] M. Noguchi *et al.*, Phys. Rev. B **62**, R9271 (2000).
[12] G. R. Blake *et al.*, Phys. Rev. Lett. **87**, 245501 (2001).
[13] S. Miyasaka *et al.*, Phys. Rev. B **68**, R100406 (2003).
[14] J.-Q. Yan *et al.*, Phys. Rev. Lett. **99**, 197201 (2007).
[15] L. D. Tung *et al.*, Phys. Rev. B **76**, 064424 (2007).
[16] J. Fujioka *et al.*, Phys. Rev. B **82**, 144425 (2010).
[17] In $R\mathrm{VO_3}$, the lattice constants show the linear dependence on the *R*-site ionic radius (Refs. 18 and 19). Assuming that Eu is trivalent, the lattice constants for $\mathrm{Eu}_{1-x}(\mathrm{La}_{0.254}\mathrm{Y}_{0.746})_x\mathrm{VO_3}$ discussed later satisfies this relationship between lattice constants and *R*-ion size. (Eu^{2+} has a much larger ionic radius than that of Eu^{3+}.) This indicates that the present system has only Eu^{3+}.
[18] M. J. Martínez-Lope *et al.*, Inorg. Chem. **47**, 2634 (2008).
[19] M. H. Sage *et al.*, Phys. Rev. B **76**, 195102 (2007).
[20] S. Miyasaka *et al.*, Phys. Rev. Lett. **99**, 217201 (2007).
[21] S. Miyasaka *et al.*, Phys. Rev. B **73**, 224436 (2006).
[22] F. Izumi and K. Momma, Solid State Phenom. **130**, 15 (2007).
[23] Y. Ren *et al.*, Phys. Rev. B **62**, 6577 (2000).
[24] At room T, the lattice constants slightly and linearly decrease with x, although the Eu^{3+} and $(\mathrm{La}_{0.254}\mathrm{Y}_{0.746})^{3+}$ have the same ionic radius. This behavior may be also induced by the change in SV.
[25] D. Bizen *et al.*, Phys. Rev. B **78**, 224104 (2008).
[26] T. Mizokawa and A. Fujimori, Phys. Rev. B **54**, 5368 (1996).
[27] T. Mizokawa, D. I. Khomskii, and G. A. Sawatzky, Phys. Rev. B **60**, 7309 (1999).
[28] S. Ishihara, Phys. Rev. B **69**, 075118 (2004).
[29] G. Khaliullin, P. Horsch, and A. M. Oleś, Phys. Rev. B **70**, 195103 (2004).
[30] Y. Motome *et al.*, Phys. Rev. Lett. **90**, 146602 (2003).
[31] S. Miyasaka *et al.*, Phys. Rev. Lett. **94**, 076405 (2005).
[32] J. Fujioka, S. Miyasaka, and Y. Tokura, Phys. Rev. B **77**, 144402 (2008).